International Journal of Cardiology 274 (2019) 27–34

Contents lists available at ScienceDirect

International Journal of Cardiology

journal homepage: www.elsevier.com/locate/ijcard

FGL2 prothrombinase contributes to the early stage of coronary microvascular obstruction through a fibrin-dependent pathway

Wen-Zhu Li [a,b,1], Yi Yang [c,1], Kun Liu [d], Rui Long [a], Nan Jin [a], Shi-Yuan Huang [a], Ya You [a], Jing Dai [a], Cheng Fan [a], Jue Wang [e,*], Zhao-Hui Wang [a,**]

[a] Department of Geriatrics, Institute of Geriatrics, Union Hospital, Tongji Medical College, Huazhong University of Science and Technology, Wuhan, China
[b] Cardiovascular Research Center, Massachusetts General Hospital, Harvard Medical School, Boston, MA, USA
[c] Department of Geriatrics, Tongji Hospital, Tongji Medical College, Huazhong University of Science and Technology, Wuhan, China
[d] Department of Cardiology, Institute of Cardiovascular Disease, Union Hospital, Tongji Medical College, Huazhong University of Science and Technology, Wuhan, China
[e] Department of Hematology, Tongji Hospital, Tongji Medical College, Huazhong University of Science and Technology, Wuhan, China

ARTICLE INFO

Article history:
Received 28 May 2018
Received in revised form 27 August 2018
Accepted 12 September 2018
Available online 13 September 2018

Keywords:
FGL2 prothrombinase
Microthrombus formation
Coronary microvascular obstruction
Fibrin deposition
Coagulation-inflammation pathway

ABSTRACT

Background: Membrane-associated fibrinogen-like protein 2 (FGL2 prothrombinase, *p*FGL2) is abundantly expressed in activated microvascular endothelial cells (MVECs) and plays a crucial role in microthrombus formation in microcirculatory vasculature. It has been widely reported that coronary microvascular obstruction (CMVO) contributes to adverse outcomes following myocardial ischemia/reperfusion. However, the role of *p*FGL2 in CMVO is poorly understood.

Methods and results: We aimed to identify the effect of MVECs-*p*FGL2 in CMVO using FGL2 knockout mice. As results, the MVECs-*p*FGL2 expression progresses significantly over 3 days and then gradually decreases, which is positively correlated with the extent of CMVO as detected by HE staining in wild type mice. Furthermore, FGL2 deficiency is correlated with decreased areas of no-reflow and necrosis as detected by Evans Blue and TTC staining and that it ameliorates cardiac dysfunction detected by hemodynamics in the early stage of CMVO. Moreover, fibrin deposition in microvasculature is significantly reduced in FGL2-deficient mice as evidenced by immunohistochemistry, MSB and Carstairs staining, along with the down-regulation of leukocyte adhesion and infiltration. Additionally, we observed that the FGL2 deficiency decreases macrophage infiltration and shifts the macrophage phenotype from pro-inflammatory (M1,) to anti-inflammatory (M2,) pattern in the early stage of CMVO.

Conclusion: These findings highlight the MVECs-*p*FGL2-fibrin pathway in the early stage of CMVO and provide insights into coagulation and inflammation for the coronary artery disease therapeutics.

1. Introduction

Coronary artery disease (CAD) is the leading medical cause of death and disability worldwide. Timely and effective primary percutaneous coronary intervention (PPCI) and thrombolytic reperfusion therapies are the preferred treatments for CAD patients who present with acute ST-elevation myocardial infarction (STEMI) [1,2]. The re-establishment of blood flow in the setting of epicardial coronary artery occlusion has saved millions of lives by limiting infarct size and ameliorating left ventricular (LV) dysfunction [1,2]. However, reperfusion therapy can be "a double-edged sword" because it can exacerbate the damage to the microvasculature, resulting in microvascular obstruction (MVO), coronary no-reflow and low or no myocardial reperfusion [3,4].

Coronary microvascular (<200 μm) obstruction (CMVO), which contributes to a lack of tissue perfusion in re-occlusion of the coronary arteries, is classified as a type of coronary "no-reflow" (CNR) phenomenon [4–6]. Increasing evidence indicates that coronary artery reflow can be increased by preventing CMVO, which improves tissue perfusion and minimizes cardiac dysfunction [3,5]. In addition to PPCI-induced "interventional CMVO" primarily caused by distal microembolization, "reperfusion MVO" is an either ischemic or infarcted region which contributes greatly to the CNR phenomenon [4,5]. Moreover, the "reperfusion CMVO" is regarded as an independent predictor of adverse clinical outcomes associated with increased mortality in acute myocardial infarction (AMI) [5]. The mechanisms involved in CMVO following ischemia and reperfusion include endothelial cell damage, microvascular thrombosis in situ, inflammatory cascade activation with leukocyte stasis

* Correspondence to: J. Wang, Department of Hematology, Tongji Hospital, Tongji Medical College, Huazhong University of Science and Technology, 1095 Jiefang Ave, Wuhan, China.
** Correspondence to: Z.H. Wang, Department of Geriatrics, Institute of Geriatrics, Union Hospital, Tongji Medical College, Huazhong University of Science and Technology, 1277 Jiefang Ave, Wuhan, China.
E-mail addresses: jeff_wangjue@hotmail.com (J. Wang), zhaohuiwang@hust.edu.cn (Z.-H. Wang).
[1] Contributed equally to this work.

https://doi.org/10.1016/j.ijcard.2018.09.051
0167-5273/

and extravasation [3,5,6]. However, the treatment of CMVO remains challenging and the precise mechanism underlying CMVO needs to be further elucidated.

Fibrinogen-like protein 2 (FGL2), also known as fibroleukin, is a multifunctional member of the fibrinogen superfamily that is involved in coagulation, cell infiltration, immunization, angiogenesis and oncogenesis [7–10]. FGL2 can function as a type II membrane-associated glycoprotein (FGL2 prothrombinase, *p*FGL2) and is abundantly expressed in activated microvascular endothelial cells (MVECs), macrophages and cancer cells, amplifying inflammatory and coagulation responses in microcirculation [9–12]. It can also present as a soluble protein that is secreted primarily by T lymphocytes participating in innate and adaptive immunity [7]. FGL2 is overexpressed in various human malignant tumors and down-regulation of FGL2 can delay tumor growth and tumor angiogenesis [9,10,13,14]. *p*FGL2 directly cleaves prothrombin to thrombin with the assistance of the phospholipids-Ca^{2+}-Va complex and subsequently initiates fibrin deposition [7,8],and is known to be a key participant in diseases associated with microcirculatory disturbances, including viral hepatitis, allograft and xenograft rejection and fetal loss syndrome [7,8]. Recently, we showed that *p*FGL2 is highly expressed in cardiac MVECs and strongly correlates with areas of no-reflow (ANR) in rats following myocardial ischemia/reperfusion (I/R) [11,15,16] as a model of CMVO [5,17].

We hypothesized that *p*FGL2 plays an important role in CMVO so that we compared FGL2-deficient mice with wild type (WT) mice subjected to myocardial I/R. Our results demonstrate that decreased expression of *p*FGL2 contributes to CMVO amelioration and *p*FGL2-fibrin pathway regulates leukocyte stasis and macrophage polarization. Therefore, *p*FGL2 deficiency may represent a novel therapeutic approach to protect against CMVO following myocardial I/R.

2. Materials and methods

2.1. Mice

WT male C57BL/6 mice were purchased from the Model Animal Research Center of Nanjing University (Nanjing, China). *Fgl2* KO mice in the C57BL/6 background were provided by Dr. Stephen T. Smiley (Trudeau Institute, Saranac Lake, NY, USA) [18]. The mice were maintained on a regular diet in a 12-h light: 12-h dark environment at 25 °C in the Animal Care Center of Tongji Medical School [19]. Heterozygous females ($fgl2^{+/-}$) were mated with heterozygous males ($fgl2^{+/-}$) to generate $fgl2^{+/+}$ and $fgl2^{-/-}$ offspring. Offspring genotypes were identified via PCR analysis. All experiments were conducted using eight- to twelve-week-old $fgl2^{+/+}$ and $fgl2^{-/-}$ male littermates.

2.2. CMVO protocol

Models of cardiac ischemia with subsequent reperfusion have been widely used to investigate the no-reflow phenomenon and CMVO [20,21]. The surgical ligation of the left anterior descending (LAD) coronary artery was performed as previously described [19,21]. Briefly, mice were anesthetized with sodium pentobarbital (50 mg/kg, P3761, Sigma) via intraperitoneal injection. The mice were shaved, intubated, connected to a rodent ventilator, and placed on a heating pad to maintain a constant body temperature. A left thoracotomy was performed at the fourth intercostal space, and the proximal LAD coronary artery was visualized and ligated using 8–0 silk sutures around a PE-10 tube. The mice were subjected to 45 min of LAD coronary occlusion followed by the removal of the suture and reperfusion for varying periods. Sham-operated mice were subjected to the same protocol except that the suture was passed under the LAD and no ligation occurred. Mice were euthanized with sodium pentobarbital (200 mg/kg) by intraperitoneal injection after the experiment, and the reperfused tissue was isolated for further assays [22].

2.3. Thioflavin S, Evans Blue and TTC staining

ANR and infarct size (IS) following the anatomical no-reflow protocol were determined as previously described [19,21,23,24]. Briefly, at different periods of reperfusion, the mice were anesthetized with sodium pentobarbital (50 mg/kg), and the hearts were then sliced into five 1-mm-thick sections along the short axis below the ligation point. ANR was evaluated via the intra-atrial injection of 1 ml/kg of a vital endothelium fluorescent dye, thioflavin S (4% solution; Sigma, MO, USA). To distinguish the ischemic zone (area at risk, AAR) from the non-ischemic zone, the LAD coronary was re-occluded, and Evans Blue dye (1% solution; Sigma, MO, USA) was injected into the left atrium. The infarct size was evaluated via 1% 2,3,5-triphenyltetrazolium chloride (TTC, St. Louis, MO, USA) solution at 37 °C for 15 min [19,20]. The sections were subsequently weighed, photographed and evaluated by using computer-assisted planimetry software (Image-Pro Plus 6.0, Media Cybermetics, MD, USA). Weights were calculated as follows: $[(R_1 \times W_1) + (R_2 \times W_2) + (R_3 \times W_3) + (R_4 \times W_4) + (R_5 \times W_5)]$, where R is the area of interest and W is the weight of the slice indicated by the subscript [19,25]. The extents of thioflavine- and TTC-negative regions were expressed as the percent of the total LV mass. The areas were determined by two observers who were blinded to each sample's identity.

2.4. Hemodynamic analysis

At different periods of reperfusion, mice were anesthetized with sodium pentobarbital (50 mg/kg) for hemodynamic measurements using a 1.4F tip micromanometer (SPR-671, Millar Instruments, TX, USA), which was inserted through the right carotid artery and proceeded further to the LV as previously described [19]. The LV end-diastolic pressure (LVEDP), the LV maximum rate of isovolumetric pressure development ($+dp/dt_{max}$) and the minimum rate of isovolumetric pressure decay ($-dp/dt_{min}$) were recorded using PowerLab equipment with Chart v5.2.1 software (ADInstruments, Castle Hill, Australia) and averaged over three consecutive cycles.

2.5. Western blot analysis

The protein level in each of the ischemic myocardium samples obtained at different periods of reperfusion were determined by Western blotting (WB) using the following primary antibodies: anti-mouse FGL2 (Abnova, Taiwan), fibrin (GeneTex, Texas, USA), Intercellular cell adhesion molecule-1 (ICAM-1, R&D System, MN, USA) and CD68 (Abcam, MA, USA). A BCA™ Protein Assay Kit (Pierce, USA) was used to determine the protein concentrations, and the weights of the protein samples were homogenized to 50 μg. Next, 30 μg were loaded per lane on a denaturing SDS 8% polyacrylamide gel. Following their transfer to nitrocellulose membranes (Invitrogen, CA, USA) that were blocked with 5% nonfat dry milk, the proteins were incubated with the above-indicated primary antibodies (0.2 μg/ml) and HRP-conjugated secondary antibodies (1:5000). Relative changes were normalized to the intensity of actin signals, and the data are expressed as percentages of the control. An ECL reagent (Pierce, IL, USA) was used for visualization, and images were recorded using a Molecular Imager ChemiDoc XRS System (Bio-Rad, CA, USA) [8,19].

2.6. Immunohistochemical analysis

Hearts were excised from the above-indicated mice, sliced transversely 4 mm from the apex, fixed in 4% paraformaldehyde and embedded as previously described [15,19]. Four-micrometer-thick sections were subjected to heat-induced epitope retrieval via immersion in 0.01 M boiling citrate buffer (pH 6.0) in a pressure cooker before cooling to room temperature and quenching with 3% H_2O_2, followed by blocking with 10% goat serum. The primary antibodies used were anti-FGL2 (Abnova, Taiwan), anti-fibrin (GeneTex, Texas, USA), anti-CD31 (Santa Cruz, CA, USA), anti-monocyte chemoattractant protein 1 (MCP-1), CD68, inducible nitric oxide synthase (iNOS) and arginase-1 (Arg-1) (Abcam, MA, USA). The signal was detected using biotin-free HRP-labeled secondary antibodies (Invitrogen, CA, USA), followed by DAB chromogen (EnVision Plus System, DAKO, Denmark). The slides were subsequently counterstained with hematoxylin and placed under coverslips. The fluorescence signal was detected with Cy3/Alexa Fluor-488-conjugated antibodies. Images were captured using Nikon Eclipse Ti-SR fluorescence microscopes. The immunostained sections were evaluated using Image-Pro Plus 6.0 by two observers who were blinded to the sample identity as described previously [26]. In brief, the quantitative values for each slide were counted by averaging the results of five representative fields (×400) in each region. First, a proportion score representing the percentage area of positive staining was calculated (0, none; 1, <1/100; 2, 1/100–1/10; 3, 1/10–1/3; 4, 1/3–2/3; 5, >2/3). Second, an intensity score representing the average intensity of the positive staining area was calculated (0, none; 1, weak; 2, intermediate; 3, strong). The proportion and intensity scores were then added to determine the total score on a scale from 0 to 8.

2.7. Histology

Four-micrometer-thick sections were prepared as detailed above. To determine differences in heart morphology, cell morphology and number of infiltrating cells among different groups, the slides were stained with HE [27]. The numbers of infiltrating cells were counted in five representative fields within each region using high-powered light microscopy (×400). Martius Scarlet Blue (MSB) and Carstairs (fibrin in red, blood cells in yellow and collagen in blue) staining are selective for fibrin as previously described [27–29]. For Carstairs staining, slides were hydrated in xylol and ethanol to distilled water, followed by incubation in 5% ferric ammonium sulfate for 5 min and staining by Mayer hematoxylin for 5 min and Picric Acid-orange G solution for 45 min. After washing, slides were stained by Ponceau Fuchsin solution for 3 min, 1% phosphotungstic acid for 3–5 min, Anilin blue solution for 10 min, and rinsed in distilled water. Slides were dehydrated covered with a coverslip using mounting medium (Pertex). All reagents were provided by EMS. Fibrin density was quantified by ImageJ as the fibrin-positive area of the total thrombus area (percentage). A proportion score representing the percentage of positive fibrin deposition was calculated as described in details above [26]. The slides were evaluated by two observers who were blinded to the sample identity.

2.8. Statistical analysis

All results are presented as means ± SEM. Data were tested for normality using the Shapiro-Wilk test. Two group comparisons of parametric data were analyzed by two-tailed Student's *t*-test, while Mann-Whitney test was used to analyzed nonparametric data. Significance between multiple groups was assessed by ANOVA with Bonferroni's post hoc analysis [8,19]. *P* values <0.05 were considered statistically significant. All statistical analyses were performed using GraphPad Prism 5.0 (GraphPad Software, CA, USA).

2.9. Study approval

Animal experiments were conducted in accordance with the recommendations of the Guide for Care and Use of Laboratory Animals of the National Institutes of Health. The protocols were approved by the Ethical Committee on Animal Experiments of Tongji Medical College, Huazhong University of Science and Technology [8].

3. Results

3.1. MVECs-pFGL2 contributes to the early-stage CMVO

Ventricular total FGL2 and microvascular *p*FGL2 expression in WT mice were evaluated via WB and immunofluorescence (IF), respectively. The WB results showed that the level of ventricular total FGL2 was the highest in the IR 3 d group (IR 1 d, IR 7 d vs IR 3 d, $^{*}P < 0.05$, n = 6; IR 1 d vs sham, $^{**}P < 0.01$, n = 6) (Fig. 1A and C). The same tendency was observed in microvascular *p*FGL2 (sham, IR 3 d vs IR 1 d, $^{**}P < 0.01$, n = 6; IR 7 d vs IR 3 d, $^{*}P < 0.05$, n = 6) (Fig. 1B and D). *p*FGL2 expression was highest in the IR 3 d group and approximately nine times higher than that of the sham group; expression was slightly decreased in the IR 7 d group (Fig. 1B and D). These findings revealed that both total FGL2 and *p*FGL2 expression reached a peak at IR 3 d in WT mice. We also evaluated the CMVO area using hematoxylin and eosin (HE) staining. As shown in Fig. 1E and F, the CMVO area was the largest in the WT IR 3 d group (WT IR 1 d, WT IR 7 d vs WT IR 3 d, $^{**}P < 0.01$, n = 6; *fgl2*$^{-/-}$ vs WT in IR 1 d, 3 d and 7 d, $^{**}P < 0.01$, $^{*}P < 0.05$, n = 6).

3.2. FGL2 deficiency decreases ANR and ameliorates cardiac dysfunction in early-stage CMVO

To investigate the relationship between microvascular *p*FGL2 expression and coronary no-reflow in the early stage, we subjected *fgl2*$^{-/-}$ mice to 45 min of ischemia and reperfusion for 1, 3 and 7 d. The knockout mice reproduced in accordance with Mendelian frequencies, appeared overtly healthy and presented normal initial numbers and proportions of lymphocytes [18]. We observed that the FGL2 deficiency was not sufficient to affect mouse cardiac morphology or function (Fig. 2 and Supplementary Fig. 1). Since FGL2 is reported to promote angiogenesis [9,10], we compared myocardial capillary density between *fgl2*$^{-/-}$ and WT mice by quantification of CD31 expression (Supplementary Methods). As results, the capillary density was decreased by approximately 28% in *fgl2*$^{-/-}$ mice in both sham and I/R 3 d group (Supplementary Fig. 2).

Thioflavin S (a fluorescent vital dye for endothelium) and Evans Blue dye were injected into the circulation to stain perfused tissue. Photographs of representative ventricular sections under ultraviolet (UV) light are presented in Fig. 2. Fig. 2A depicts the non-ischemic area, the AAR and the ANR. The navy blue-stained tissue represents the non-ischemic area; the green-stained remainder was defined as the AAR, and the regions within the AAR that failed to stain green were considered as the ANR (Fig. 2A and B). The AAR/LV ratios were not significantly different among the groups (Fig. 2D), indicating that the ligation site of LAD was the same in each group. In contrast, the ANR/LV ratios reached a peak in the WT IR 3 d group (22.6 ± 1.3%; WT IR 1 d, WT IR 7 d vs WT

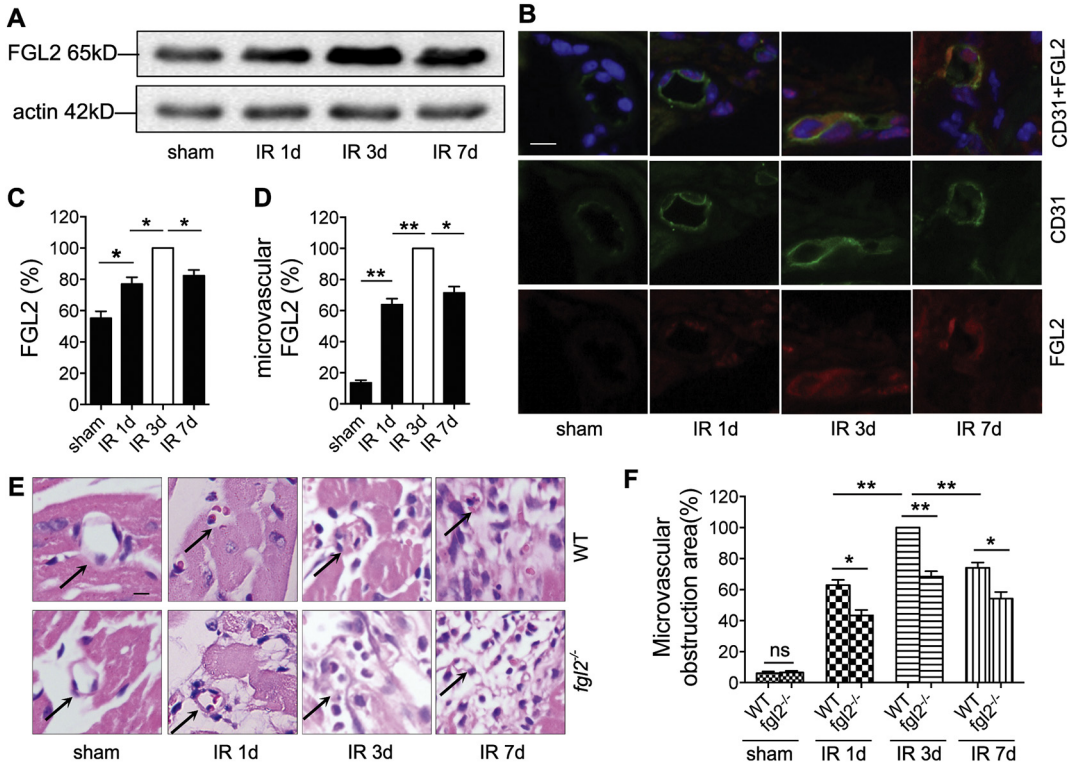

Fig. 1. MVECs-*p*FGL2 contributes in early-stage CMVO. (A) Representative ventricular total FGL2 expression levels in WT by WB. (B) Representative microvascular *p*FGL2 expression levels in WT by double immunofluorescence staining. The MVECs were stained with CD31 (green) and *p*FGL2 (red), and nuclei were stained with DAPI (blue). Scale bar, 10 μm. (C) Quantification of (A) (n = 6). (D) Quantification of (B) (n = 6). (E) Representative images of CMVO evaluated by HE staining in WT and *fgl2*$^{-/-}$ mice. The black arrows indicate CMVO, and the black bar represents 10 μm. (F) Quantification of (E) (n = 6). Data are presented as the mean ± SEM normalized to the WT IR 3 d group from three independent experiments (ANOVA, $^{*}P < 0.05$, $^{**}P < 0.01$; ns, not significant).

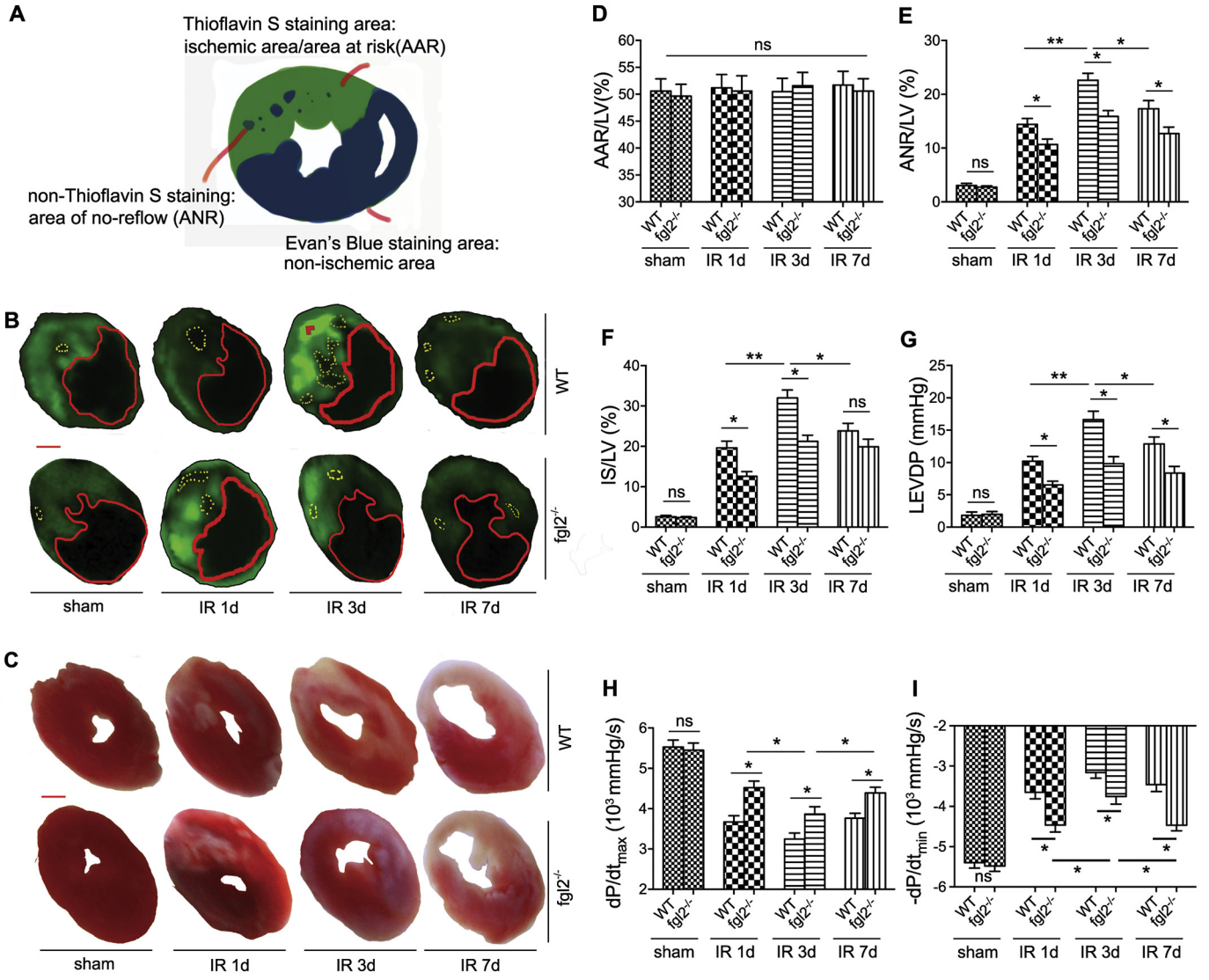

Fig. 2. FGL2 deficiency decreases ANR and ameliorates cardiac dysfunction in early-stage CMVO. (A) Schematic diagram showing a transverse heart slide of thioflavin S and Evans Blue staining followed ischemia and reperfusion. The navy blue-stained tissue represents a non-ischemic area, the green-stained tissue represents the area at risk (AAR), and regions within the AAR exhibiting darker color represent area of no-reflow (ANR). (B) Representative cross-sections of hearts from WT and *fgl2*$^{-/-}$ mice subjected to IR 1 d, IR 3 d and IR 7 d detected by thioflavin S and Evans Blue staining. Area encircled by red line indicates the non-ischemic area, green area indicates the AAR, and yellow area, which is represented by a dashed line, indicates the ANR. Scale bar, 200 μm. (C) Representative cross-sections of hearts from WT and *fgl2*$^{-/-}$ mice detected by TTC staining. The infarct area is in white, and the non-infarct area is in red. Scale bar, 200 μm. (D) Quantification of (B) AAR/LV ratios (n = 6). (E) Quantification of (B) ANR/LV ratios (n = 6). (F) Quantification of (C) IS/LV ratios (n = 6). (G) LVEDP was detected by hemodynamics (n = 6). (H and I) LV cardiac function (dP/dt_{max}, $-dP/dt_{min}$) was detected by hemodynamics (n = 6). Data are presented as the mean ± SEM normalized to the WT IR 3 d group from three independent experiments (ANOVA, $^{*}P < 0.05$, $^{**}P < 0.01$; ns, not significant).

IR 3 d, $^{**}P < 0.01$, $^{*}P < 0.05$, n = 6; *fgl2*$^{-/-}$ vs WT in IR 1 d, 3 d and 7 d, $^{*}P < 0.05$, n = 6) (Fig. 2E), indicating that the proportion of the microvasculature salvaged during reperfusion was smallest in the WT IR 3 d group and that the deletion of FGL2 salvaged the microvasculature in the early stage.

In addition, TTC staining was used to measure the IS, which is presented in Fig. 2C. Viable myocardium presents as brick red, whereas necrosis appears as white. Compared with ANR/LV, the same tendency was observed in IS/LV in the IR 1 d and IR 3 d groups, but no significant difference was observed in the IR 7 d group (Fig. 2F).

To determine the effect of *fgl2* deficiency on cardiac hemodynamic parameters, we measured the LVEDP and dP/dt. The LEVDP reached a peak in the WT IR 3 d group (16.6 ± 1.3 mm Hg; WT IR 1 d, WT IR 7 d vs WT IR 3 d, $^{**}P < 0.01$, $^{*}P < 0.05$, n = 6; *fgl2*$^{-/-}$ vs WT in IR 1 d, 3 d and 7 d, $^{*}P < 0.05$, n = 6) (Fig. 2G). The same pattern was observed in dP/dt_{max} and $-dP/dt_{min}$ (Fig. 2H and I). These results indicated that the deletion of FGL2 increased LV diastolic and systolic function.

3.3. pFGL2 deficiency decreases fibrin deposition in-situ in early-stage CMVO

Bursts of fibrin deposition are associated with CMVO and lead to a reduction in blood flow. To investigate the mechanism responsible for CMVO in FGL2-deficient mice, we examined fibrin deposition at 3 d following I/R via WB and fibrin-specific pathological staining. WB analysis revealed that FGL2 deficiency reduced fibrin deposition significantly (Fig. 3A and B). IHC, Carstairs and MSB staining revealed fibrin deposition in the microvasculature (Fig. 3C). Intra-microvascular fibrin deposition was also found to be significantly decreased in the *fgl2*$^{-/-}$ groups (WT IR 3 d vs *fgl2*$^{-/-}$ IR 3 d, $^{**}P < 0.01$, n = 6) (Fig. 3D). These findings

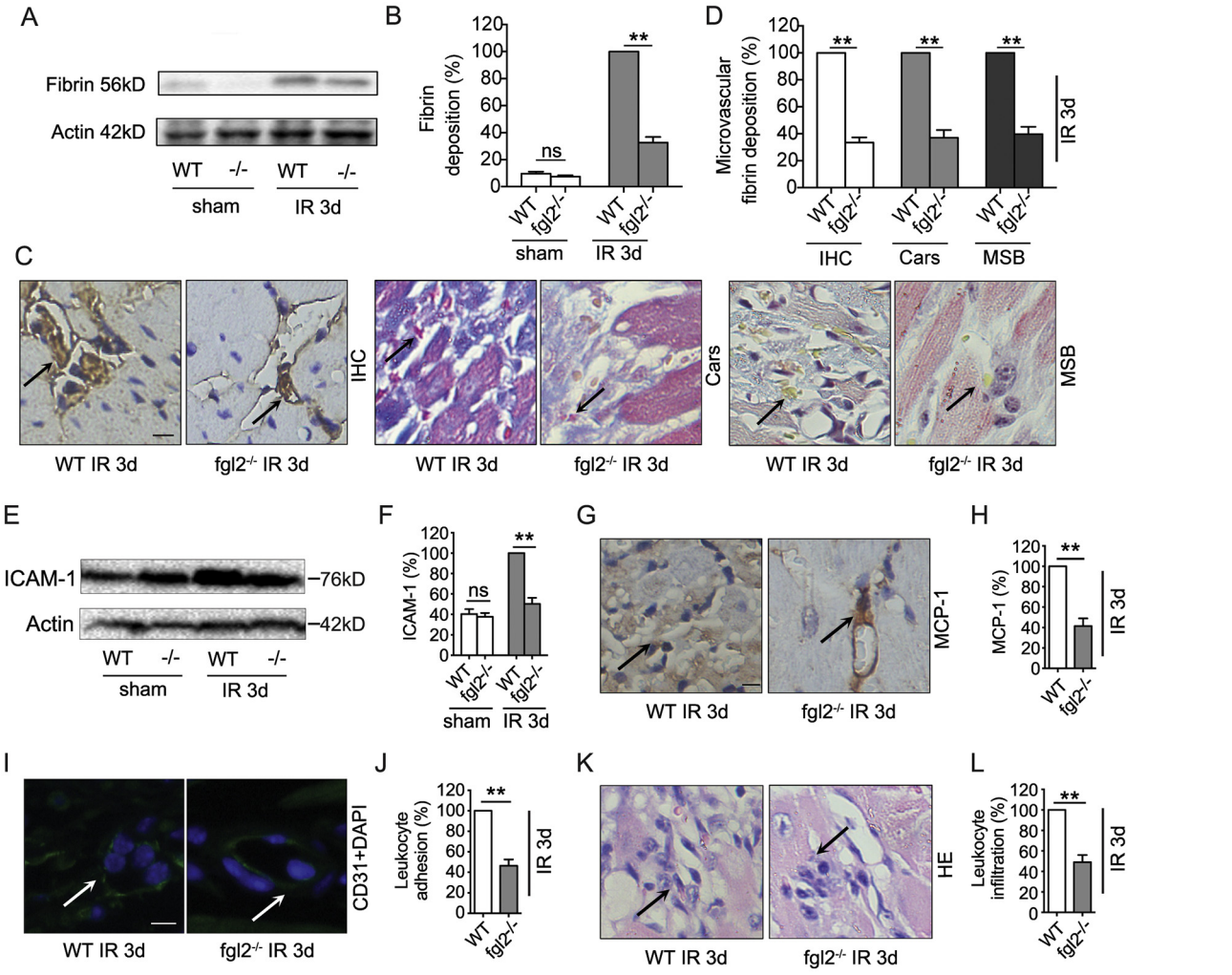

Fig. 3. *p*FGL2 deficiency decreases fibrin deposition in-situ and attenuates leukocyte adhesion and infiltration in early-stage CMVO. (A) Representative ventricular total fibrin deposition in WT and *fgl2*$^{-/-}$ *group* by WB. (B) Quantification of (A) (n = 6). (C) Microvascular fibrin deposition by IHC, Carstairs and MSB staining. Black arrows indicate fibrin deposition in microvasculars. Scale bar, 40 μm. (D) Quantitative analysis of (C) (n = 6). (E) Representative intercellular ICAM-1 expression levels in LV tissues by WB. (F) Quantification of (E) (n = 6). (G) Representative MCP-1 expression levels by IHC. (H) Quantification of (G) (n = 6). (I) Representative leukocyte adhesion in microvasculars by Immunofluorescence staining. MVECs were stained with CD31 (green), and nuclei were stained with DAPI (blue). White arrows indicate microvasculars. Scale bar, 10 μm. (J) Quantification of (I) (n = 6). (K) Representative leukocyte infiltration by HE staining. Black arrows indicate leukocyte infiltration. Scale bar, 10 μm. (L) Quantification of (K) (n = 6). Data are presented as the mean ± SEM normalized to the WT IR 3 d group from three independent experiments (unpaired Student's *t*-test for two groups; ANOVA for multiple groups; $^{**}P < 0.01$; ns, not significant).

revealed that *p*FGL2 deficiency suppressed both total and intra-microvascular fibrin deposition following I/R.

3.4. FGL2 deficiency attenuates leukocyte adhesion and infiltration in early-stage CMVO

The cleavage of fibrinogen to fibrin results in the rapid expression and exposure of chemokines and adhesive proteins involved in leukocyte recruitment and adhesion [30,31]. To investigate the downstream effects of fibrin in FGL2-deficient mice, we measured the levels of adhesive protein ICAM-1, MCP-1, leukocyte adhesion and infiltration. WB analysis revealed that FGL2 deficiency significantly reduced the expression of ICAM-1 at IR 3 d (WT IR 3 d vs *fgl2*$^{-/-}$ IR 3 d, $^{**}P < 0.01$, n = 6) (Fig. 3E and F). IHC analysis showed that FGL2 deficiency significantly reduced the expression of MCP-1 at IR 3 d (WT IR 3 d vs *fgl2*$^{-/-}$ IR 3 d, $^{**}P < 0.01$, n = 6) (Fig. 3G and H). IF analysis showed that leukocyte adhesion in the microvasculature was significantly decreased in the *fgl2*$^{-/-}$ groups (WT IR 3 d vs *fgl2*$^{-/-}$ IR 3 d, $^{**}P < 0.01$, n = 6) (Fig. 3I and J). HE staining revealed that FGL2 deficiency reduced leukocyte infiltration (WT IR 3 d vs *fgl2*$^{-/-}$ IR 3 d, $^{**}P < 0.01$, n = 6) (Fig. 3K and L).

3.5. FGL2 deficiency decreases macrophage infiltration and shifts the macrophage phenotype from M1 to M2 in early-stage CMVO

Two major macrophage activation patterns contribute to inflammation and repair processes in myocardial ischemia/reperfusion injury: classical (M1, pro-inflammatory) and alternative (M2, anti-inflammatory) [32,33]. To investigate the role of *p*FGL2 on the polarization of the infiltrated macrophage phenotype, the expression of CD68 (macrophage marker), iNOS (M1 macrophage marker) and Arg-1 (M2 macrophage marker) was detected by WB and IF. WB analysis revealed that the protein level of CD68 was significantly reduced in the *fgl2*$^{-/-}$ group compared with the WT group (WT IR 3 d vs *fgl2*$^{-/-}$ IR 3 d, $^{**}P < 0.01$, n = 6) (Fig. 4A and B), indicating that FGL2 deficiency decreases the amount of macrophage infiltration. IF staining showed that the iNOS/CD68 ratio was significantly reduced in the *fgl2*$^{-/-}$ group compared with the WT group (WT IR 3 d vs *fgl2*$^{-/-}$ IR 3 d, $^{**}P < 0.01$, n = 6) (Fig. 4C and D), whereas the Arg-1/CD68 ratio was significantly higher in the *fgl2*$^{-/-}$ group than in the WT group (WT IR 3 d vs *fgl2*$^{-/-}$ IR 3 d, $^{**}P < 0.01$, n = 6) (Fig. 4E and F).

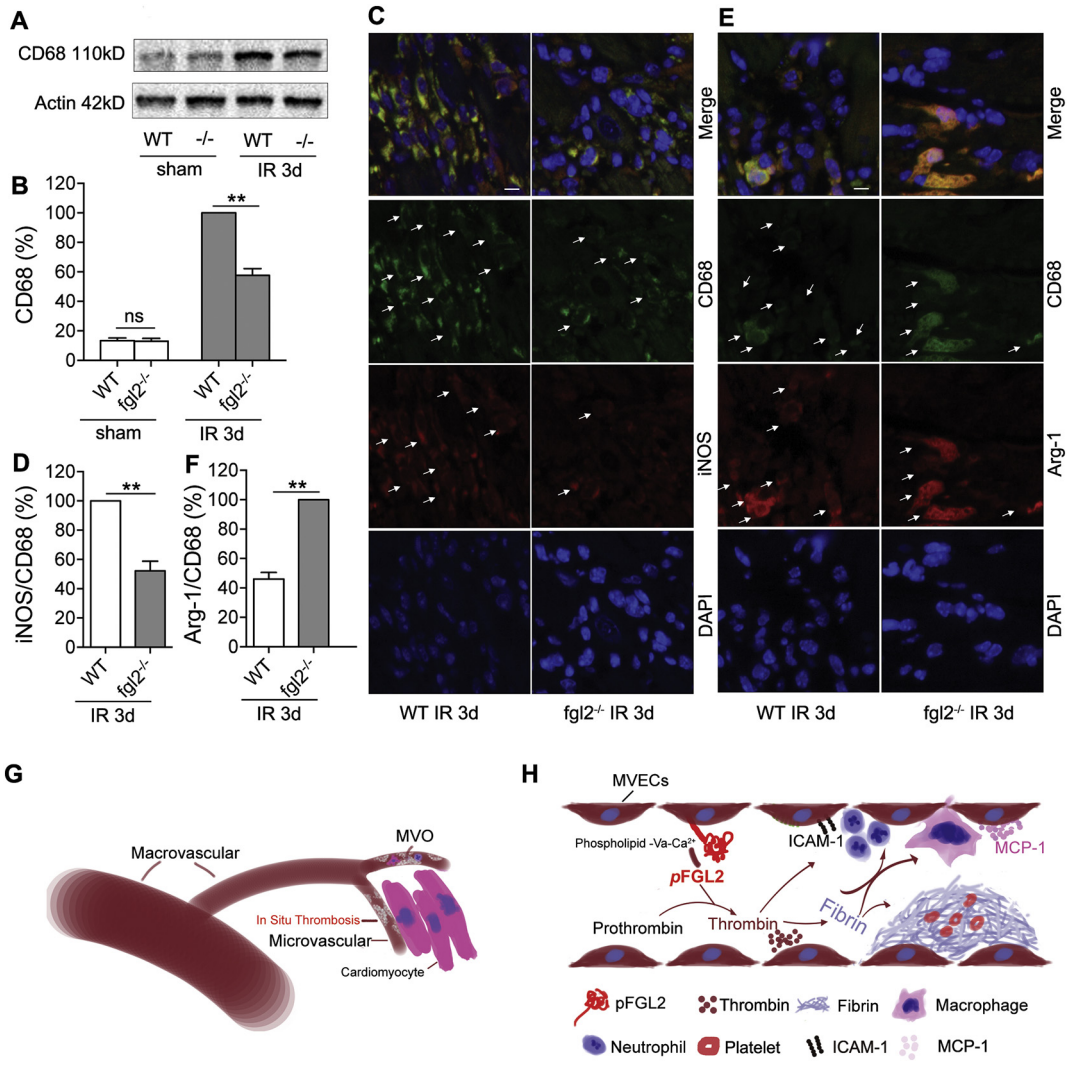

Fig. 4. FGL2 deficiency decreases macrophage infiltration and shifts the macrophage phenotype from M1 to M2 in early-stage CMVO. (A) Representative macrophage marker CD68 level in LV tissues by WB. (B) Quantification of (A) (n = 6). (C) Representative iNOS positive in the infiltrated macrophages by double immunofluorescence staining. Macrophages were stained with CD68 (green) and iNOS (red), and nuclei were stained with DAPI (blue). Scale bar, 10 μm. (D) Quantification of (C) (n = 6). (E) Representative Arg-1 positive in the infiltrated macrophages by double immunofluorescence staining. Macrophages were stained with CD68 (green) and Arg-1 (red), and nuclei were stained with DAPI (blue). Scale bar, 10 μm. (F) Quantification of (E) (n = 6). (G and H) Schematic diagram of the contribution of the MVECs-*p*FGL2-fibrin pathway in early-stage CMVO. Data are presented as the mean ± SEM normalized to the WT IR 3 d group from three independent experiments (unpaired Student's *t*-test for two groups; ANOVA for multiple groups; $^{**}P < 0.01$; ns, not significant).

4. Discussion

This study demonstrated that MVECs-*p*FGL2 expression might contribute to CMVO via fibrin in-situ deposition as well as via the leukocyte activation and macrophage polarization during the development of cardiac dysfunction. Our results provide new insights into the mechanisms underlying coronary no-reflow phenomenon.

We addressed several important issues in this study. First, the present study is the first to utilize genetically FGL2 knocked-out mice in the experimental CMVO model and to demonstrate that FGL2 deficiency ameliorates ANR, IS and cardiac dysfunction in the early stage of CMVO in vivo. Second, we showed that FGL2-deletion significantly decreases fibrin deposition in situ and immediately induce the CMVO improvement. Third, we observed that FGL2 deficiency was strongly associated with a multitude of down-regulated pro-inflammatory cytokines, suggesting that pro-coagulation and immuno-regulation ability both contribute to FGL2's role in the CMVO.

Traditional "anatomical" no-reflow models have been widely used to study the CMVO following myocardial I/R injury [17]. Thus, to explore the FGL2's role in CMVO in vivo, genetically engineered FGL2 knockout mice were considered as appropriate models [18]. However, one concern regarding the engineered FGL2 knockout mice is that the ablation of FGL2 may cause neonatal death or impaired immune activity [34,35]. Interestingly, the FGL2-deficient mice in present study exhibited comparable cardiac morphology, cardiac function and immune activity to the wild-type control (Fig. 2 and Supplementary Fig. 1). This discrepancy may arise from the different methodology applied in generating FGL2 knockout mice because it is possible that the forced expression of β-galactosidase from a *LacZ* insertion in mice genome may result in neonatal toxicity during embryogenesis [18]. Yet we still observed decreased capillary density in FGL2 knockout mice independent of I/R injury, in accordance with previous reports that FGL2 promotes angiogenesis [9,10]. It is possible that less capillary density in heart and reduced coagulation activity both contribute to reduced fibrin deposition observed in FGL2 knockout mice. On the other hand, lowered capillary density appears to be an adverse effect to I/R injury [36]. Therefore, the overall amelioration of cardiac dysfunction in FGL2-deficient mice indicate that inhibition of pro-inflammatory effects as well as coagulation activity of FGL2 may compensate for reduced myocardial capillaries. Other methods, such as conditional knockout mice or blocking

antibody of FGL2, may help to rule out the anatomical difference of capillary density in future study.

Of note, the FGL2-deficiency is associated with significantly decreased ANR/LV percentage as well as decreased IS/LV percentage from 1 to 3 day post myocardial I/R injury in our study. Since the no-reflow area is always smaller than, and contained within, the infarcted region, it remains unclear whether the better LV function is solely dealing with the ameliorated CMVO or due to the smaller total IS area. However, the incidence and extent of early-stage CMVO have been shown to be strong predictors for cardiac dysfunction, adverse left ventricular remodeling and worse outcome in long-term studies. Thorsten R et al. [37] reported that the no-reflow phenomenon persists for 1 month after myocardial I/R in rats and predicts infarct expansion. This is partially corroborated by findings from Matthijs van K et al. [38] in a pooled meta-analysis of 1025 patients, that CMVO detected by magnetic resonance is associated with cardiac death when adjusted for age and LVEF, whereas IS/LV percentage was not an independent predictor of major adverse cardiovascular events or cardiac death when adjusted for CMVO and LVEF. Thus, the decreased ANR/LV observed in FGL2-deficient mice may exert long-term protective effects post myocardial I/R and further investigation is needed.

It has been well established that the *p*FGL2-fibrin pathway plays a critical role in microcirculatory disturbance-associated diseases, such as allograft/xenograft rejection, viral hepatitis, fetal loss syndrome and type 2 diabetic nephropathy [39–42]. Our previous work [42] suggested that FGL2 may activate renal microthrombosis and play a role in renal microangiopathy of rats with type 2 diabetes. Mendicino et al. [39] reported that in a cardiac xenotransplantation model, graft hearts from $fgl2^{-/-}$ donors had less fibrin deposition than wild-type donors during acute vascular rejection. It is noteworthy that the process of acute vascular rejection, similar to coronary no reflow, also involves intravascular thrombosis, fibrin deposition and endothelial cell activation. Interestingly, although >60% reduction in fibrin deposition in-situ was achieved in the present study, we still observed remaining fibrin deposition in the $fgl2^{-/-}$ group (Fig. 3), suggesting that other coagulation factors, such as tissue factor [43], might contribute to fibrin deposition. Moreover, our previous study demonstrate that TNF-α upregulates FGL2 expression mediating the formation of fibrin-rich microthrombus in cardiac microvascular endothelial cells (CMEC) during I/R injury [11]. Similar findings described by *Zheng ZZ* et al [44] point out that FGL2 gene silencing reduces the TNF-α levels and improves hearts function of STZ-induced diabetes rats. Thus, pro-inflammatory cytokines such as TNF-α play important roles in the pro-coagulation and immunoregulation process of FGL2. Taking together, our results corroborate with previous reports showing that fibrin serves as a pivotal link between thrombosis and pro-inflammatory responses, both of which greatly contribute to the progression of CMVO and cardiac dysfunction [31].

In conclusion, our results provide the first evidence that FGL2 prothrombinase plays a crucial role via the *p*FGL2-fibrin pathway in mice subjected to myocardial I/R. Novel agents targeting *p*FGL2 without influencing classical coagulation cascades may serve as a potential clinical approach to protect against CMVO.

Funding

This work was supported in part by the National Natural Science Foundation of China [No. 81270267 to ZHW, 81501209 to WZL] and the Doctoral Supervisory Foundation of Ministry of Education of China [No. 20130142110067 to ZHW].

Acknowledgments

We thank Dr. Stephen T. Smiley for providing *Fgl2* KO mice, Dr. Liang Tang and Liang Deng for their expert technical assistance, and Dr. Hasseb Satter and Sanaz Darbalaei for manuscript improvement.

Conflict of interest disclosures

None declared.

Appendix A. Supplementary data

Supplementary data to this article can be found online at https://doi.org/10.1016/j.ijcard.2018.09.051.

References

[1] P.G. Steg, S.K. James, D. Atar, L.P. Badano, C.B. Lundqvist, M.A. Borger, C. Di Mario, K. Dickstein, G. Ducrocq, F. Fernandez-Aviles, A.H. Gershlick, P. Giannuzzi, S. Halvorsen, K. Huber, P. Juni, A. Kastrati, J. Knuuti, M.J. Lenzen, K.W. Mahaffey, M. Valgimigli, A. Van'T Hof, P. Widimsky, D. Zahger, J.J. Bax, H. Baumgartner, C. Ceconi, V. Dean, C. Deaton, R. Fagard, C. Funck-Brentano, D. Hasdai, A. Hoes, P. Kirchhof, P. Kolh, T. McDonagh, C. Moulin, B.A. Popescu, Ž. Reiner, U. Sechtem, P.A. Sirnes, M. Tendera, A. Torbicki, A. Vahanian, S. Windecker, F. Astin, K. Åström-Olsson, A. Budaj, P. Clemmensen, J.P. Collet, K.A. Fox, A. Fuat, O. Gustiene, C.W. Hamm, P. Kala, P. Lancellotti, A. Pietro Maggioni, B. Merkely, F.J. Neumann, M.F. Piepoli, F. Van De Werf, F. Verheugt, L. Wallentin, ESC Guidelines for the management of acute myocardial infarction in patients presenting with ST-segment elevation, Eur. Heart J. (2012) https://doi.org/10.1093/eurheartj/ehs215.

[2] P.T. O'Gara, F.G. Kushner, D.D. Ascheim, D.E. Casey, M.K. Chung, J.A. de Lemos, S.M. Ettinger, J.C. Fang, F.M. Fesmire, B.A. Franklin, C.B. Granger, H.M. Krumholz, J.A. Linderbaum, D.A. Morrow, L.K. Newby, J.P. Ornato, N. Ou, M.J. Radford, J.E. Tamis-Holland, C.L. Tommaso, C.M. Tracy, Y.J. Woo, D.X. Zhao, 2013 ACCF/AHA guideline for the management of ST-elevation myocardial infarction: a report of the American College of Cardiology Foundation/American Heart Association Task Force on Practice Guidelines, Circulation (2013) https://doi.org/10.1161/CIR.0b013e3182742cf6.

[3] B.G. Schwartz, R.A. Kloner, Coronary no reflow, J. Mol. Cell. Cardiol. (2012) https://doi.org/10.1016/j.yjmcc.2011.06.009.

[4] G. Niccoli, F. Burzotta, L. Galiuto, F. Crea, Myocardial no-reflow in humans, J. Am. Coll. Cardiol. (2009) https://doi.org/10.1016/j.jacc.2009.03.054.

[5] R. Jaffe, A. Dick, B.H. Strauss, Prevention and treatment of microvascular obstruction-related myocardial injury and coronary no-reflow following percutaneous coronary intervention: a systematic approach, JACC Cardiovasc. Interv. (2010) https://doi.org/10.1016/j.jcin.2010.05.004.

[6] S. Limalanathan, J. Eritsland, G.Ø. Andersen, N.E. Kløw, M. Abdelnoor, P. Hoffmann, Myocardial salvage is reduced in primary PCI-treated STEMI patients with microvascular obstruction, demonstrated by early and late CMR, PLoS One (2013) https://doi.org/10.1371/journal.pone.0071780.

[7] H. Liu, P.S. Yang, T. Zhu, J. Manuel, J. Zhang, W. He, I. Shalev, L. Zhang, M.I. Cybulsky, D.R. Grant, M.J. Phillips, G.A. Levy, Characterization of fibrinogen-like protein 2 (FGL2): monomeric FGL2 has enhanced immunosuppressive activity in comparison to oligomeric FGL2, Int. J. Biochem. Cell Biol. 45 (2013) 408–418, https://doi.org/10.1016/j.biocel.2012.10.014.

[8] W.Z. Li, J. Wang, R. Long, G.H. Su, D.K. Bukhory, J. Dai, N. Jin, S.Y. Huang, P. Jia, T. Li, C. Fan, K. Liu, Z. Wang, Novel antibody against a glutamic acid-rich human fibrinogen-like protein 2-derived peptide near Ser91 inhibits hfgl2 prothrombinase activity, PLoS One 9 (2014) https://doi.org/10.1371/journal.pone.0094551.

[9] E. Rabizadeh, I. Cherny, D. Lederfein, S. Sherman, N. Binkovsky, Y. Rosenblat, A. Inbal, The cell-membrane prothrombinase, fibrinogen-like protein 2, promotes angiogenesis and tumor development, Thromb. Res. 136 (2015) 118–124, https://doi.org/10.1016/j.thromres.2014.11.023.

[10] Y. Liu, L. Xu, Q. Zeng, J. Wang, M. Wang, D. Xi, X. Wang, D. Yang, X. Luo, Q. Ning, Downregulation of FGL2/prothrombinase delays HCCLM6 xenograft tumour growth and decreases tumour angiogenesis, Liver Int. 32 (2012) 1585–1595, https://doi.org/10.1111/j.1478-3231.2012.02865.x.

[11] P. Jia, J. Wang, L. Wang, X. Chen, Y. Chen, W.Z. Li, R. Long, J. Chen, Y.W. Shu, K. Liu, Z.H. Wang, TNF-α upregulates Fgl2 expression in rat myocardial ischemia/reperfusion injury, Microcirculation 20 (2013) 524–533, https://doi.org/10.1111/micc.12050.

[12] Y. Liu, S. Xu, F. Xiao, Y. Xiong, X. Wang, S. Gao, W. Yan, Q. Ning, The FGL2/fibroleukin prothrombinase is involved in alveolar macrophage activation in COPD through the MAPK pathway, Biochem. Biophys. Res. Commun. (2010) https://doi.org/10.1016/j.bbrc.2010.04.145.

[13] M. Tang, X. Cao, P. Li, K. Zhang, Y. Li, Q.-Y. Zheng, G.-Q. Li, J. Chen, G.-L. Xu, K.-Q. Zhang, Increased expression of fibrinogen-like protein 2 is associated with poor prognosis in patients with clear cell renal cell carcinoma OPEN, Sci. Rep. (2017) 1–10, https://doi.org/10.1038/s41598-017-13149-x.

[14] M. Wang, J. Liu, D. Xi, X. Luo, Q. Ning, Adenovirus-mediated artificial miRNA against human fibrinogen like protein 2 inhibits hepatocellular carcinoma growth, J. Gene Med. (2016) https://doi.org/10.1002/jgm.2883.

[15] L. Shao, Y. Zhang, A. Ma, P. Zhang, D. Wu, W. Li, J. Wang, K. Liu, Z. Wang, Atorvastatin preconditioning improves the forward blood flow in the no-reflow rats, Fundam. Clin. Pharmacol. (2014) https://doi.org/10.1111/j.1472-8206.2012.01074.x.

[16] L. Shao, D. Wu, P. Zhang, W. Li, J. Wang, G. Su, Y. Liao, Z. Wang, K. Liu, The significance of microthrombosis and fgl2 in no-reflow phenomenon of rats with acute myocardial ischemia/reperfusion, Clin. Appl. Thromb. Hemost. 19 (2013) 19–28, https://doi.org/10.1177/1076029612437577.

[17] T.K.R. Reffelmann, Microvascular Obstruction: The No-Reflow Phenomenon in Animal Models of Myocardial Ischemia and Reperfusion, Springer, London, 2012.
[18] W.W. Hancock, F.M. Szaba, K.N. Berggren, M.A. Parent, I.K. Mullarky, J. Pearl, A.M. Cooper, K.H. Ely, D.L. Woodland, I.J. Kim, M.A. Blackman, L.L. Johnson, S.T. Smiley, Intact type 1 immunity and immune-associated coagulative responses in mice lacking IFN gamma-inducible fibrinogen-like protein 2, Proc. Natl. Acad. Sci. U. S. A. (2004) https://doi.org/10.1073/pnas.0308369101\r0308369101 (pii).
[19] Y.H. Liao, N. Xia, S.F. Zhou, T.T. Tang, X.X. Yan, B.J. Lv, S.F. Nie, J. Wang, Y. Iwakura, H. Xiao, J. Yuan, H. Jevallee, F. Wei, G.P. Shi, X. Cheng, Interleukin-17A contributes to myocardial ischemia/reperfusion injury by regulating cardiomyocyte apoptosis and neutrophil infiltration, J. Am. Coll. Cardiol. (2012) https://doi.org/10.1016/j.jacc.2011.10.863.
[20] Y. Liu, K. Lian, L. Zhang, R. Wang, F. Yi, C. Gao, C. Xin, D. Zhu, Y. Li, W. Yan, L. Xiong, E. Gao, H. Wang, L. Tao, TXNIP mediates NLRP3 inflammasome activation in cardiac microvascular endothelial cells as a novel mechanism in myocardial ischemia/reperfusion injury, Basic Res. Cardiol. (2014) https://doi.org/10.1007/s00395-014-0415-z.
[21] C. Gandhi, D.G. Motto, M. Jensen, S.R. Lentz, A.K. Chauhan, ADAMTS13 deficiency exacerbates VWF-dependent acute myocardial ischemia/reperfusion injury in mice, Blood (2012) https://doi.org/10.1182/blood-2012-06-440255.
[22] M. Du, K. Huang, D. Huang, L. Yang, L. Gao, X. Wang, D. Huang, X. Li, C. Wang, F. Zhang, Y. Wang, M. Cheng, Q. Tong, G. Qin, K. Huang, L. Wang, Renalase is a novel target gene of hypoxia-inducible factor-1 in protection against cardiac ischaemia-reperfusion injury, Cardiovasc. Res. (2015) https://doi.org/10.1093/cvr/cvu255.
[23] S. Blum, R. Asaf, J. Guetta, R. Miller-Lotan, R. Asleh, R. Kremer, N.S. Levy, F.G. Berger, D. Aronson, X. Fu, R. Zhang, S.L. Hazen, A.P. Levy, Haptoglobin genotype determines myocardial infarct size in diabetic mice, J. Am. Coll. Cardiol. (2007) https://doi.org/10.1016/j.jacc.2006.08.044.
[24] A. Martire, B. Fernandez, A. Buehler, C. Strohm, J. Schaper, R. Zimmermann, P.E. Kolattukudy, W. Schaper, Cardiac overexpression of monocyte chemoattractant protein-1 in transgenic mice mimics ischemic preconditioning through SAPK/JNK1/2 activation, Cardiovasc. Res. (2003) https://doi.org/10.1016/S0008-6363(02)00697-1.
[25] T. Izumi, Y. Saito, I. Kishimoto, M. Harada, K. Kuwahara, I. Hamanaka, N. Takahashi, R. Kawakami, Y. Li, G. Takemura, H. Fujiwara, D.L. Garbers, S. Mochizuki, K. Nakao, Blockade of the natriuretic peptide receptor guanylyl cyclase-A inhibits NF-κB activation and alleviates myocardial ischemia/reperfusion injury, J. Clin. Invest. (2001) https://doi.org/10.1172/JCI12088.
[26] M.C. Lloyd, K.O. Alfarouk, D. Verduzco, M.M. Bui, R.J. Gillies, M.E. Ibrahim, J.S. Brown, R.A. Gatenby, Vascular measurements correlate with estrogen receptor status, BMC Cancer (2014) https://doi.org/10.1186/1471-2407-14-279.
[27] A.F. Stein-Merlob, C.W. Kessinger, S. Sibel Erdem, H. Zelada, S.A. Hilderbrand, C.P. Lin, G.J. Tearney, M.R. Jaff, G.L. Reed, P.K. Henke, J.R. McCarthy, F.A. Jaffer, Blood accessibility to fibrin in venous thrombosis is thrombus age-dependent and predicts fibrinolytic efficacy: an in vivo fibrin molecular imaging study, Theranostics (2015) https://doi.org/10.7150/thno.12494.
[28] G. Hornstra, Dietary Fats, Prostanoids and Arterial Thrombosis, Springer Science & Business Media, 2011.
[29] K.C. Carstairs, The identification of platelets and platelet antigens in histological sections, J. Pathol. Bacteriol. (1965) https://doi.org/10.1002/path.1700900124.
[30] D. Chen, A. Carpenter, J. Abrahams, R.C. Chambers, R.I. Lechler, J.H. McVey, A. Dorling, Protease-activated receptor 1 activation is necessary for monocyte chemoattractant protein 1–dependent leukocyte recruitment in vivo, J. Exp. Med. (2008) https://doi.org/10.1084/jem.20071427.
[31] P. Petzelbauer, P.A. Zacharowski, Y. Miyazaki, P. Friedl, G. Wickenhauser, F.J. Castellino, M. Gröger, K. Wolff, K. Zacharowski, The fibrin-derived peptide Bβ15–42 protects the myocardium against ischemia-reperfusion injury, Nat. Med. (2005) https://doi.org/10.1038/nm1198.
[32] C. Troidl, H. Möllmann, H. Nef, F. Masseli, S. Voss, S. Szardien, M. Willmer, A. Rolf, J. Rixe, K. Troidl, S. Kostin, C. Hamm, A. Elsässer, Classically and alternatively activated macrophages contribute to tissue remodelling after myocardial infarction, J. Cell. Mol. Med. (2009) https://doi.org/10.1111/j.1582-4934.2009.00707.x.
[33] N.G. Frangogiannis, The inflammatory response in myocardial injury, repair, and remodelling, Nat. Rev. Cardiol. (2014) https://doi.org/10.1038/nrcardio.2014.28.
[34] R. Khattar, O. Luft, N. Yavorska, I. Shalev, M.J. Phillips, O. Adeyi, D. Gao, A. Bartczak, P. Urbanellis, W. Shyu, J. Zhang, J. Manuel, G.A. Levy, N. Selzner, Targeted deletion of FGL2 leads to increased early viral replication and enhanced adaptive immunity in a murine model of acute viral hepatitis caused by LCMV WE, PLoS One 8 (2013) https://doi.org/10.1371/journal.pone.0072309.
[35] J. Mu, D. Qu, A. Bartczak, M.J. Phillips, J. Manuel, W. He, C. Koscik, M. Mendicino, L. Zhang, D. a Clark, D.R. Grant, P.H. Backx, G.A. Levy, S.L. Adamson, J. Mu, D. Qu, A. Bartczak, P. Mj, J. Manuel, W. He, M. Mendicino, L. Zhang, C. Da, B. Ph, Fgl2 deficiency causes neonatal death and cardiac dysfunction during embryonic and postnatal development in mice, Physiol. Genomics (2007) 53–62, https://doi.org/10.1152/physiolgenomics.00026.2007.
[36] M. Prech, S. Grajek, A. Marszalek, M. Lesiak, M. Jemielity, A. Araszkiewicz, T. Mularek-Kubzdela, A. Cieslinski, Chronic infarct-related artery occlusion is associated with a reduction in capillary density. Effects on infarct healing, Eur. J. Heart Fail. (2006) https://doi.org/10.1016/j.ejheart.2005.10.016.
[37] T. Reffelmann, S.L. Hale, J.S. Dow, R.A. Kloner, No-reflow phenomenon persists long-term after ischemia/reperfusion in the rat and predicts infarct expansion, Circulation (2003) https://doi.org/10.1161/01.CIR.0000101917.80668.E1.
[38] M. Van Kranenburg, M. Magro, H. Thiele, S. DeWaha, I. Eitel, A. Cochet, Y. Cottin, D. Atar, P. Buser, E. Wu, D. Lee, V. Bodi, G. Klug, B. Metzler, R. Delewi, P. Bernhardt, W. Rottbauer, E. Boersma, F. Zijlstra, R.J. Van Geuns, Prognostic value of microvascular obstruction and infarct size, as measured by CMR in STEMI patients, JACC Cardiovasc. Imaging (2014) https://doi.org/10.1016/j.jcmg.2014.05.010.
[39] M. Mendicino, M.F. Liu, A. Ghanekar, W. He, C. Koscik, I. Shalev, M. Javadi, J. Turnbull, W. Chen, L. Fung, S. Sakamoto, P. Marsden, T.K. Waddell, M.J. Phillips, R. Gorczynski, G.A. Levy, D. Grant, Targeted deletion of Fgl-2/fibroleukin in the donor modulates immunologic response and acute vascular rejection in cardiac xenografts, Circulation (2005) https://doi.org/10.1161/CIRCULATIONAHA.105.534271.
[40] A. Ghanekar, M. Mendicino, H. Liu, W. He, M. Liu, R. Zhong, M.J. Phillips, G. a Levy, D.R. Grant, Endothelial induction of fgl2 contributes to thrombosis during acute vascular xenograft rejection, J. Immunol. (2004) https://doi.org/10.4049/jimmunol.172.9.5693.
[41] P.A. Marsden, Q. Ning, L.S. Fung, X. Luo, Y. Chen, M. Mendicino, A. Ghanekar, J.A. Scott, T. Miller, C.W.Y. Chan, M.W.C. Chan, W. He, R.M. Gorczynski, D.R. Grant, D.A. Clark, M.J. Phillips, G.A. Levy, The Fgl2/fibroleukin prothrombinase contributes to immunologically mediated thrombosis in experimental and human viral hepatitis, J. Clin. Invest. (2003) https://doi.org/10.1172/JCI18114.
[42] G. Su, K. Liu, Y. Wang, J. Wang, X. Li, W. Li, Y. Liao, Z. Wang, Fibrinogen-like protein 2 expression correlates with microthrombosis in rats with type 2 diabetic nephropathy, J. Biomed. Res. 25 (2011) 120–127, https://doi.org/10.1016/S1674-8301(11)60015-8.
[43] S.M. Day, J.L. Reeve, B. Pedersen, D.M. Farris, D.D. Myers, M. Im, T.W. Wakefield, N. Mackman, W.P. Fay, Macrovascular thrombosis is driven by tissue factor derived primarily from the blood vessel wall, Blood (2005) https://doi.org/10.1182/blood-2004-06-2225.
[44] Z. Zhengzhong, Y. Yafa, L. Jin, Fibrinogen-like protein 2 gene silencing inhibits cardiomyocytes apoptosis, improves heart function of streptozotocin—induced diabetes rats and the molecular mechanism involved, Biosci. Rep. (2015) 1–7, https://doi.org/10.1042/BSR20150078.